



Published in final edited form as:

*Mol Imaging Biol.* 2018 October ; 20(5): 835–845. doi:10.1007/s11307-018-1170-6.

## Evaluation of Pancreatic VMAT2 Binding with Active and Inactive Enantiomers of [<sup>18</sup>F]FP-DTBZ in Healthy Subjects and Patients with Type 1 Diabetes

Mika Naganawa<sup>1</sup>, Keunpoong Lim<sup>1</sup>, Nabeel B. Nabulsi<sup>1</sup>, Shu-fei Lin<sup>1</sup>, David Labaree<sup>1</sup>, Jim Ropchan<sup>1</sup>, Kevan C. Herold<sup>1</sup>, Yiyun Huang<sup>1</sup>, Paul Harris<sup>2</sup>, Masanori Ichise<sup>2</sup>, Gary W. Cline<sup>1</sup>, and Richard E. Carson<sup>1</sup>

<sup>1</sup>Yale University, P.O. Box 208048, New Haven, CT, 06520-8048, USA

<sup>2</sup>Columbia University, New York, NY, USA

### Abstract

**Purpose**—Previous studies demonstrated the utility of [<sup>18</sup>F]fluoropropyl-(+)-dihydrotrabenazine ([<sup>18</sup>F]FP-(+)-DTBZ) as a positron emission tomography (PET) radiotracer for the vesicular monoamine transporter type 2 (VMAT2) to quantify beta cell mass in healthy control (HC) and type 1 diabetes mellitus (T1DM) groups. Quantification of specific binding requires measurement of non-displaceable uptake. Our goal was to identify a reference tissue (renal cortex or spleen) to quantify pancreatic non-specific binding of [<sup>18</sup>F]FP-(+)-DTBZ with the inactive enantiomer, [<sup>18</sup>F]FP-(-)-DTBZ. This was the first human study of [<sup>18</sup>F]FP-(-)-DTBZ.

**Procedures**—Six HCs and four T1DM patients were scanned on separate days after injection of [<sup>18</sup>F]FP-(+)-DTBZ or [<sup>18</sup>F]FP-(-)-DTBZ. Distribution volumes ( $V_T$ ) and standardized uptake values (SUVs) were compared between groups. Three methods for calculation of non-displaceable uptake ( $V_{ND}$ ) or reference SUV were applied: (1) use of [<sup>18</sup>F]FP-(+)-DTBZ reference  $V_T$  as  $V_{ND}$ , assuming  $V_{ND}$  is uniform across organs; (2) use of [<sup>18</sup>F]FP-(-)-DTBZ pancreatic  $V_T$  as  $V_{ND}$ , assuming that  $V_{ND}$  is uniform between enantiomers in the pancreas; and (3) use of a scaled [<sup>18</sup>F]FP-(+)-DTBZ reference  $V_T$  as  $V_{ND}$ , assuming that a ratio of non-displaceable uptake between organs is uniform between enantiomers. Group differences in  $V_T$  (or SUV), binding potential ( $BP_{ND}$ ), or SUV ratio (SUVR) were estimated using these three methods.

---

*Correspondence to:* Mika Naganawa; mika.naganawa@yale.edu.

Compliance with Ethical Standards

Conflict of Interest

The authors declare that they have no conflict of interest.

Ethical Approval

All procedures performed in studies involving human participants were in accordance with the ethical standards of the institutional and/or national research committee and with the 1964 Helsinki Declaration and its later amendments or comparable ethical standards. This study was approved by the Yale University Human Investigation Committee and the Yale-New Haven Hospital Radiation Safety Committee.

Informed Consent

Informed consent was obtained from all patients included in this study.

Electronic supplementary material The online version of this article (<https://doi.org/10.1007/s11307-018-1170-6>) contains supplementary material, which is available to authorized users.

**Results**— $[^{18}\text{F}]\text{FP}(-)\text{-DTBZ}$   $V_T$  values were different among organs, and  $V_T(+)$  and  $V_T(-)$  were also different in the renal cortex and spleen. Method 3 with the spleen to estimate  $V_{\text{ND}}$  (or reference SUV) gave the highest non-displaceable uptake and the largest HC vs. T1DM group differences. Significant group differences were also observed in  $V_T$  (or SUV) with method 1 using spleen. SUV was affected by differences in the input function between groups and between enantiomers.

**Conclusions**—Non-displaceable uptake was different among organs and between enantiomers. Use of scaled spleen  $V_T$  values for  $V_{\text{ND}}$  is a suitable method for quantification of VMAT2 in the pancreas.

### Keywords

Vesicular monoamine transporter type 2; PET;  $[^{18}\text{F}]\text{FP}(+)\text{-DTBZ}$ ;  $[^{18}\text{F}]\text{FP}(-)\text{-DTBZ}$ ; Pancreas non-displaceable uptake

### Introduction

The radiotracer  $[^{18}\text{F}]\text{fluoropropyl}(+)\text{-dihydrotrabenazine}$  ( $[^{18}\text{F}]\text{FP}(+)\text{-DTBZ}$ ) is a positron emission tomography (PET) imaging agent for the vesicular monoamine transporter type 2 (VMAT2). In addition to the brain, VMAT2 is expressed within the pancreas [1–3], and its pancreatic distribution strongly correlated and overlapped with the insulin-positive  $\beta$ -cell [4], with a minor (7–10 %) [4–6] contribution from VMAT2-positive pancreatic polypeptide (PP) cells. Therefore,  $[^{18}\text{F}]\text{FP}(+)\text{-DTBZ}$  has been evaluated as a possible biomarker to quantify human beta cell mass (BCM). If VMAT2-positive PP cells are not affected by T1DM, the total specific binding of  $[^{18}\text{F}]\text{FP}(+)\text{-DTBZ}$  in the T1DM group would be only 7–10 % of that in healthy control (HC) group.

$[^{18}\text{F}]\text{FP}(+)\text{-DTBZ}$  shows excellent pancreatic uptake in rodents [7], baboons [5, 8], and humans [9, 10]. Additionally,  $[^{18}\text{F}]\text{FP}(+)\text{-DTBZ}$  binding in the pancreas was significantly reduced in patients with type 1 diabetes mellitus (T1DM), compared with HCs. Given that functional BCM in T1DM patients should be nearly depleted, the reduction in  $[^{18}\text{F}]\text{FP}(+)\text{-DTBZ}$  binding was smaller than might be expected. Since the PET signal is a sum of specific VMAT2 binding in the  $\beta$ -cells, minor specific binding to the PP cells, and non-displaceable uptake (*i.e.*, non-specific binding + free tracer in pancreatic tissue), current PET imaging data suggest that some or all of the signals in T1DM patients were due to non-specific uptake.

To address this hypothesis, the pancreatic non-displaceable uptake of  $[^{18}\text{F}]\text{FP}(+)\text{-DTBZ}$  must be known. Non-displaceable uptake in the rodent pancreas was estimated as ~ 20 % of the total by pre-treatment [7] or ~ 40 % by displacement [11] with unlabeled  $\text{FP}(+)\text{-DTBZ}$ . Non-displaceable uptake can also be estimated if a suitable reference tissue with minimal specific VMAT2 signal can be defined. Such an ideal reference tissue would have uptake equal to the non-displaceable uptake in the pancreas. From previous baboon studies, it is not clear if such an ideal reference exists.

Non-displaceable distribution volume ( $V_{ND}$ ) in baboons was assessed with active (+)- and inactive (-)-enantiomers of [ $^{18}\text{F}$ ]FP-DTBZ [5, 8], taking advantage of the large differences in stereospecific affinity, i.e.,  $K_i$  of  $> 3000 \text{ nM}$  for the (-)-enantiomer vs.  $0.1 \text{ nM}$  for the (+)-enantiomer [12]. For simplification, the distribution volumes ( $V_T$ ) of [ $^{18}\text{F}$ ]FP-(+)-DTBZ and [ $^{18}\text{F}$ ]FP-(-)-DTBZ are indicated as  $V_{T(+)}$  and  $V_{T(-)}$ , respectively. Similarly,  $V_{ND}$  values are indicated as  $V_{ND(+)}$  and  $V_{ND(-)}$ . Harris et al. found that  $V_{T(+)}$  of the renal cortex and spleen were similar to the  $V_{T(-)}$  of the pancreas [8], suggesting that pancreatic  $V_{ND(+)}$  could be estimated by  $V_{T(+)}$  of the renal cortex or spleen. In contrast, our study showed that the  $V_{T(+)}$  values of the renal cortex and spleen differed and were higher than the  $V_{T(-)}$  of the pancreas by 125 % (renal cortex) and 30 % (spleen) [5]. In addition,  $V_{T(-)}$  values among the pancreas, renal cortex, and spleen differed, indicating that non-specific uptake was different among the organs, and there was no ideal reference tissue. We therefore assessed three methods to define pancreatic  $V_{ND}$ : (1)  $V_{T(+)}$  in the renal cortex or spleen, (2)  $V_{T(-)}$  in the pancreas, and (3) a scaled  $V_{T(+)}$  in the renal cortex or spleen [5]. We also evaluated the presence of tissue radiometabolites with an *ex vivo* study [5] in baboons and showed that radiometabolites in the spleen and pancreas were low (6 and  $\sim 1$  %, respectively) but were more dominant in the renal cortex (30 %). Thus, the spleen was regarded as a more favorable candidate for a pseudo-reference tissue.

In this study, we extended our baboon work and conducted PET studies of [ $^{18}\text{F}$ ]FP-(+)-DTBZ and [ $^{18}\text{F}$ ]FP-(-)-DTBZ in HCs and T1DM patients. Our goal was to identify a suitable reference tissue or normalizing method to quantify specific pancreatic binding of [ $^{18}\text{F}$ ]FP-(+)-DTBZ and to assess whether any methods for  $V_{ND}$  calculation would be appropriate for both HC and T1DM subjects.

## Materials and Methods

### Human Subjects

Six HC subjects (20–35 years; five males and one female;  $85.9 \pm 8.8 \text{ kg}$ ;  $\text{BMI} = 27.2 \pm 8.8 \text{ kg/m}^2$ ) and four T1DM patients (28–36 years; three males and one female;  $77.2 \pm 6.7 \text{ kg}$ ;  $\text{BMI} = 25.8 \pm 1.0 \text{ kg/m}^2$ ; duration of diabetes = 12–29 years; C-peptide  $< 0.1 \text{ ng/ml}$ ; insulin dose ( $n = 2$ ) = 30–40 U/day) were recruited for this study. The BMI of the HC group was more variable than that of the T1DM group. Each subject was scanned twice on different days, after injection of either [ $^{18}\text{F}$ ]FP-(+)-DTBZ or [ $^{18}\text{F}$ ]FP-(-)-DTBZ. This IRB-approved study was also approved by the Yale-New Haven Hospital Radiation Safety Committee and an exploratory Investigational New Drug (eIND) application for [ $^{18}\text{F}$ ]FP-(-)-DTBZ was approved by the FDA. All subjects provided written consent. The study was performed in accordance with federal guidelines and regulations of the USA for the protection of human research subjects contained in Title 45 Part 46 of the Code of Federal Regulations (45 CFR 46).

### Synthesis of [ $^{18}\text{F}$ ]FP-(+)-DTBZ and [ $^{18}\text{F}$ ]FP-(-)-DTBZ

[ $^{18}\text{F}$ ]FP-(+)-DTBZ and [ $^{18}\text{F}$ ]FP-(-)-DTBZ were synthesized as described in [5]; see supplemental material.

Radiochemical purity of the final product was > 97 %. Specific activities of [ $^{18}\text{F}$ ]FP-(+)-DTBZ and [ $^{18}\text{F}$ ]FP-(-)-DTBZ were  $260 \pm 129$  MBq/nmol ( $n=10$ ) and  $293 \pm 112$  MBq/nmol ( $n=10$ ), respectively, at the end of synthesis.

### Arterial Input Function Measurement

For the first 7 min of each study, arterial blood was continuously counted for radioactivity using an automated system (PBS-101; Veenstra Instruments, Joure, The Netherlands). Discrete blood samples were manually drawn at 3, 5, 7, 15, 20, 30, 45, 60, 75, 90, and 120 min. Samples were centrifuged to obtain plasma, and then whole blood and plasma samples were counted with a calibrated well counter.

Analysis of the parent and its metabolites in the plasma by HPLC and measurement of plasma free fraction ( $f_p$ ) of the radiotracers were conducted following procedures described before [5].

### PET Imaging and Image Processing

For most scans, the radiotracer was administered over 1 min by an infusion pump. Four subjects (one HC and three T1DM) had previously been scanned with [ $^{18}\text{F}$ ]FP-(+)-DTBZ using bolus plus constant infusion (B/I) ( $K_{\text{bol}} = 360$  min), and their B/I PET data were converted to bolus data using the Eq. 5B in [13], in order to compare the standard uptake values (SUVs) obtained using different tracer injection protocols. PET images were acquired for 2 h using a Biograph mCT PET/x-ray computed tomography (CT) scanner (Siemens Medical Solutions, Knoxville, TN). Dynamic data were reconstructed with the ordered subset expectation maximization algorithm with point spread function correction using time-of-flight measurements. Frame timing was  $6 \times 30$  s,  $3 \times 1$  min,  $2 \times 2$  min, and  $22 \times 5$  min.

PET images were corrected for motion using a mutual information algorithm (Bioimage Suite, version 3.01, [www.bioimagesuite.com](http://www.bioimagesuite.com)) and registered to a moving average reference image. The first reference image was obtained by summing the first 10 min of data (initial frame subset), and the next frame was realigned to this reference image. Then, the subset used to compute the reference image was updated by replacing the first frame with the motion-corrected frame. This process was repeated over the whole dataset.

### Computation of Regional Time-Activity Curves

Regions of interest (ROIs) of the pancreas, renal cortex, and spleen were manually delineated on multiple slices of the summed (0–90 min post injection) motion-corrected images. To minimize partial volume and respiratory motion effects, the ROIs were thinned using the *classical thinning algorithm* [14] and skeletonized to one voxel (2 mm) thickness. Typical examples of ROIs are shown in Fig. S1 (supplemental material). The algorithm uses morphological image processing, preserving the topology (extent and connectivity) of the original ROI. The final ROIs were applied to generate time-activity curves (TACs).

### Kinetic Modeling and Non-displaceable Distribution Volume Estimation

Outcome measures were derived with kinetic analysis of the TACs using the metabolite-corrected input function. The one- and two-tissue compartment (1TC, 2TC) models and the

multilinear analysis 1 (MA1) method ( $t^*=40$  min) [15] were applied to calculate the distribution volume ( $V_T$ ) [16]. The MA1 method uses the arterial input function to calculate two parameters,  $V_T$  and  $b$  (constant value after an equilibration time,  $t^*$ ). The renal cortex and spleen have been proposed as reference tissue candidates, and our baboon displacement study suggested that these regions lack specific binding [5]. Assuming that [ $^{18}\text{F}$ ]FP(-)-DTBZ uptake in all regions and [ $^{18}\text{F}$ ]FP(+)-DTBZ uptake in non-pancreatic regions do not contain specific binding, we applied three methods to define  $V_{\text{ND}}$ :

1. The spleen was used as a reference tissue as in previous reports, *i.e.*, using  $V_T(+)$  in the spleen as  $V_{\text{ND}}(+)$  in the pancreas.
2. Pancreatic  $V_T(-)$  was assumed to be  $V_{\text{ND}}(+)$  in the pancreas. Note that a pair of scans (with [ $^{18}\text{F}$ ]FP(+)-DTBZ and [ $^{18}\text{F}$ ]FP(-)-DTBZ) would be required for each subject.
3.  $V_{\text{ND}}$  was allowed to be non-uniform across tissues for the enantiomers, but it was assumed that the ratios of  $V_{\text{ND}}$  in the non-pancreas regions to that in the pancreas are constant between the two enantiomers. For example, the ratio  $V_{\text{ND}}(-,\text{spleen})/V_{\text{ND}}(-,\text{pancreas})$ ,  $\alpha_{\text{spleen}}$ , was assumed to be equal to the ratio  $V_{\text{ND}}(+,\text{spleen})/V_{\text{ND}}(+,\text{pancreas})$ . Therefore,  $V_{\text{ND}}(+,\text{pancreas})$  was estimated as  $V_T(+,\text{spleen})/\alpha_{\text{spleen}}$ , where the ratio,  $\alpha_{\text{spleen}}$ , was determined by using the  $V_T$  values of the [ $^{18}\text{F}$ ]FP(-)-DTBZ scan. If the scaling factor,  $\alpha_{\text{spleen}}$ , is reproducible across scans and subjects, [ $^{18}\text{F}$ ]FP(-)-DTBZ scans are not required.

Methods 1 and 3 were also assessed using the renal cortex as a reference tissue. Using each method to derive  $V_{\text{ND}}$ ,  $BP_{\text{nd}}$  was determined as  $V_T/V_{\text{ND}} - 1$ , and the group difference between the HC and T1DM was assessed.

### Assessment of Standardized Uptake Value

SUVs were computed over the time window, 60–120 min. The B/I PET data were converted to bolus values for SUV computation (see “Discussion” for details). The pancreas and spleen TACs of T1DM patients before and after conversion are shown in the supplementary material (Fig. S2). The SUV ratio (SUVR), the ratio of SUV in the pancreas to that in the reference tissue, was determined with the reference SUV calculated using methods 1 and 3. The group differences of SUV and SUVR were compared with those of  $V_T$  and  $BP_{\text{ND}}$  to investigate the potential use of SUV and SUVR.

### Statistical Analysis

Outcome measures were compared between HC and T1DM groups using two-tailed Student's  $t$  test and two-tailed nonparametric test (Mann-Whitney test and Wilcoxon matched-pairs signed-rank test). Since  $P$  values were similar between parametric and non-parametric tests and significance ( $P < 0.05$ ) did not change between the tests, parametric test results are shown in the “Results.” All modeling was performed with in-house programs written with IDL 8.0 (ITT Visual Information Solutions, Boulder, CO).

## Results

### Human Injection and Scan Parameters

Injection parameters are summarized in Table 1. The injected mass and specific activity did not differ between the scans with [<sup>18</sup>F]FP-(+)-DTBZ and [<sup>18</sup>F]FP-(-)-DTBZ (paired *t* test, *P* = 0.24 and *P* = 0.37) or between HC and T1DM groups for each radiotracer (unpaired *t* test, *P* = 0.38 and *P* = 0.93 for [<sup>18</sup>F]FP-(+)-DTBZ and *P* = 0.90 and *P* = 0.79 for [<sup>18</sup>F]FP-(-)-DTBZ). The average free fractions were significantly different (paired *t* test, *P* < 0.001).

### Plasma Analysis

Figure 1 shows the unmetabolized fractions for [<sup>18</sup>F]FP-(+)-DTBZ and [<sup>18</sup>F]FP-(-)-DTBZ across all scans, and sample chromatographs for each tracer. Parent fractions for [<sup>18</sup>F]FP-(+)-DTBZ and [<sup>18</sup>F]FP-(-)-DTBZ were 39 ± 16 and 38 ± 11 % at 60 min post injection, respectively. The unmetabolized fractions were similar between [<sup>18</sup>F]FP-(+)-DTBZ and [<sup>18</sup>F]FP-(-)-DTBZ, while the chromatograms showed different metabolite profiles. For both radiotracers, the unmetabolized fractions were similar between HC and T1DM groups, while the metabolite-corrected plasma SUV curves were higher in the HC than in the T1DM group (Fig. 2). In both groups, [<sup>18</sup>F]FP-(-)-DTBZ plasma SUV curves were higher than those of [<sup>18</sup>F]FP-(+)-DTBZ.

### Uptake of the Enantiomers

Figures 3 and 4 show SUV images and regional TACs for [<sup>18</sup>F]FP-(+)-DTBZ and [<sup>18</sup>F]FP-(-)-DTBZ. Uptake of [<sup>18</sup>F]FP-(-)-DTBZ in all regions peaked at 3–5 min post injection and then rapidly decreased in both HC and T1DM groups. Similar uptake patterns were seen with [<sup>18</sup>F]FP-(+)-DTBZ in the renal cortex and spleen. As shown previously, pancreatic uptake of [<sup>18</sup>F]FP-(+)-DTBZ reached its peak at around 30 min post injection and cleared slowly.

### Kinetic Model Assessment

For both enantiomers, the quality of curve fitting was similarly good with the 2TC and MA1 models (Fig. 4), while a moderate lack of fit was seen with the 1TC model. The 2TC  $V_T$  estimates were not always stable ( $V_T > 1000$  ml/cm<sup>3</sup>, relative standard error > 10 %; unstable results in ~ 15 % of all fits). Using the 2TC values as a gold standard (excluding unstable estimates), the 1TC  $V_T$  values showed substantial underestimation for [<sup>18</sup>F]FP-(+)-DTBZ ( $V_{T(1TC)} = 0.74 \times V_{T(2TC)} + 2.00$ ,  $R^2 = 0.95$ ). The slope of the regression line was close to 1 for [<sup>18</sup>F]FP-(-)-DTBZ ( $V_{T(1TC)} = 1.03 \times V_{T(2TC)} - 2.22$ ,  $R^2 = 0.95$ ); however, the 1TC  $V_T$  values showed substantial underestimation in the kidney region ( $V_{T(1TC,kidney)} = 0.40 \times V_{T(2TC,kidney)} + 2.72$ ,  $R^2 = 0.43$ ). MA1  $V_T$  values showed a much smaller discrepancy with respect to the 2TC for both enantiomers ([<sup>18</sup>F]FP-(+)-DTBZ:  $V_{T(MA1)} = 0.89 \times V_{T(2TC)} + 4.88$ ,  $R^2 = 1.00$ ; [<sup>18</sup>F]FP-(-)-DTBZ:  $V_{T(MA1)} = 0.92 \times V_{T(2TC)} + 1.41$ ,  $R^2 = 0.98$ ). The underestimation in the kidney for [<sup>18</sup>F]FP-(-)-DTBZ was also improved using the MA1 method ( $V_{T(MA1,kidney)} = 0.82 \times V_{T(2TC,kidney)} + 2.75$ ,  $R^2 = 0.77$ ). Given the good quality of fit, estimation with good stability, and moderate underestimation, the MA1 model was chosen as the model to compute  $V_T$  values. Table 2 and Fig. 5 show  $V_T$  values and



SUVs from 60 to 120 min post injection. For both radiotracers,  $V_T$  and SUVs were highest in the pancreas. For [ $^{18}\text{F}$ ]FP-(+)-DTBZ,  $V_T$  and SUVs in the spleen were higher than those in the renal cortex ( $V_T$ :  $P=0.032$  (HC),  $P=0.004$  (T1DM); SUV:  $P=0.018$  (HC),  $P=0.086$  (T1DM)). For [ $^{18}\text{F}$ ]FP-(-)-DTBZ,  $V_T$  and SUVs in the spleen were similar to those in the renal cortex ( $V_T$ :  $P=0.19$  (HC),  $P=0.46$  (T1DM); SUV:  $P=0.18$  (HC),  $P=0.47$  (T1DM)). Blood volume correction was not included in the above modeling. To assess if this correction was necessary, the 1TC and 2TC models with blood volume correction were also applied to the TACs. For the renal cortex, the fitted blood volume value was implausible ( $>100\%$ ) in most scans regardless of the model. Using the 1TC model, the fitted blood volume values differed greatly among scans in the pancreas (0~113% for [ $^{18}\text{F}$ ]FP-(+)-DTBZ and 0~105% for [ $^{18}\text{F}$ ]FP-(-)-DTBZ) and in the spleen (26~181% for [ $^{18}\text{F}$ ]FP-(+)-DTBZ and 10~108% for [ $^{18}\text{F}$ ]FP-(-)-DTBZ). Using the 2TC model, the blood volume also varied over scans in the pancreas (0~51% for [ $^{18}\text{F}$ ]FP-(+)-DTBZ and 0~57% for [ $^{18}\text{F}$ ]FP-(-)-DTBZ) and spleen (0~82% for [ $^{18}\text{F}$ ]FP-(+)-DTBZ and 8~62% for [ $^{18}\text{F}$ ]FP-(-)-DTBZ). In summary, the blood volume could not be estimated reliably based on the kinetic analyses of these radiotracers. Therefore, we used fixed blood volume values taken from the literature (pancreas 27% [17], spleen 63% [18], and kidney 17% [18]) when applying the MA1 model to the TACs. The estimated results are shown in the supplementary material (Tables S1 and S2). The estimated distribution volumes were reduced by a small amount (a reduction of 0–2 ml/cm<sup>3</sup>). The delay between the plasma input curve and tissue time-activity curves was not taken into account in the modeling. It is expected that the delay has a negligible effect on  $V_T$  values. To investigate the effect of delay, we computed the  $V_T$  values using the MA1 model with delay. The delay was estimated by applying the 1TC model to the first 10-min whole-body TAC. As expected, the  $V_T$  values did not change ( $V_T(\text{MA1 with delay}) = 0.99 \times V_T(\text{MA1 without delay}) + 0.08$ ,  $R^2 = 1.00$ ).

$V_T(+)$  and SUV(+) values in the pancreas were also compared between HC and T1DM groups. As expected, a significant group difference was found ( $V_T$ :  $P=0.04$ ; SUV:  $P=0.002$ ) with differences of 42% for  $V_T$  and 56% for SUV.

SUV(-) values in the pancreas were significantly higher in the HC than in the T1DM group, and at least some of these differences were attributed to input function effects (see “Discussion”). SUV(+) and SUV(-) values in the renal cortex and spleen were also higher in the HC than in the T1DM group, but the difference was not significant.  $V_T(-)$  values in the pancreas were higher in the HC, but this difference was not significant. The  $V_T(+)$  and  $V_T(-)$  values in the renal cortex and spleen did not show group differences.

### Non-displaceable Binding Estimation

Table 3 summarizes the  $V_{ND}$  and pancreatic  $BP_{ND}$  estimates using the three methods with two different reference tissues. In method 1, which uses the reference tissue  $V_T(+)$  values, a significant group difference was found ( $P=0.01$ ) in pancreas  $BP_{nd}$  with the spleen reference, but not with the renal reference. Method 2 used pancreatic  $V_T(-)$  as  $V_{ND}$ , and since this value was similar to or lower than  $V_T(+)$  in the renal cortex or spleen, method 2 gave similar or higher  $BP_{ND}$  values compared to method 1. Additionally, the group difference in  $BP_{ND}$  using method 2 was smallest among all methods. For method 3, which

accounts for the inter-organ differences in  $V_T(-)$  by scaling the  $V_T(+)$  values in the reference tissues, the scale factor ( $\alpha$ ) was not significantly different between HC and T1DM groups. Therefore, the whole population value ( $\alpha$ ) was used to calculate  $V_{ND}(+)$ . Pancreatic  $BP_{ND}$  using method 3 was smaller than that from other methods, since the calculated  $V_{ND}(+)$  was larger. The group difference in  $BP_{nd}$  using the method 3 with  $\alpha_{spleen}$  was largest (75 %) among all methods. Method 3 yielded large inter-subject variability (COV) in the T1DM group, since  $BP_{nd}$  values were very low.

The reference SUV and SUVR-1 values are summarized in Table 4 (SUVR-1 is shown to be compatible with  $BP_{nd}$ ). Overall, the results showed similar patterns to the  $V_{ND}$  and  $BP_{nd}$  estimates. Significant group differences were found in methods 1 and 3, with the spleen as a reference tissue, and the  $P$  values were smaller when SUVR, rather than  $BP_{nd}$ , was used. The largest group difference was found in method 3 with  $\alpha_{spleen}$ . We selected methods 1 and 3 with the spleen as a reference tissue for normalization.

## Discussion

PET studies were conducted with two radiolabeled enantiomers, [ $^{18}\text{F}$ ]FP-(+)-DTBZ and [ $^{18}\text{F}$ ]FP-(-)-DTBZ, in HCs and T1DM patients. Our hypothesis was that [ $^{18}\text{F}$ ]FP-(-)-DTBZ enables a direct measurement of non-displaceable uptake for quantitative imaging with [ $^{18}\text{F}$ ]FP-(+)-DTBZ. We evaluated three normalizing methods to quantify the specific binding of [ $^{18}\text{F}$ ]FP-(+)-DTBZ in the pancreas. To the best of our knowledge, this was the first PET imaging study of [ $^{18}\text{F}$ ]FP-(-)-DTBZ in humans.

To compute the SUV obtained using different tracer injection protocols (B/I and bolus), the B/I PET data were converted to bolus data using the equation in [13]. Since the biological system is linear at tracer doses, the B/I response can be determined from the response function of a bolus injection, and the B/I SUVs can be accurately corrected to the bolus SUVs. This process accounts for the fact that the unmetabolized fraction from the B/I PET data will be higher than that from the bolus PET data. Kinetic parameters other than SUV are not affected by the difference in the injection protocols.

Active and inactive enantiomers of [ $^{11}\text{C}$ ]DTBZ have been used to measure non-displaceable uptake and to assess VMAT2-specific binding in the human brain [19]. The distribution of [ $^{11}\text{C}$ ](-)-DTBZ was moderately uniform across the brain. However, it was not clear yet whether enantiomers of [ $^{18}\text{F}$ ]FP-DTBZ can be used to measure pancreatic non-displaceable uptake and assess whether non-displaceable uptake is uniform across organs. A baboon study by Harris et al. [8] reported the pancreatic  $V_T(-)$  was similar to  $V_T(+)$  in both the spleen and kidney, indicating that the spleen and kidney might be suitable reference tissues. However, we found heterogeneous  $V_T(-)$  among organs in baboons [5], suggesting the absence of an ideal reference tissue in non-human primates [5].

Comparing  $V_T$  values between baboons [5] and humans, pancreas  $V_T(+)$  and  $V_T(-)$  and spleen  $V_T(+)$  were similar. While  $V_T(-)$  was highest in the renal cortex in baboon, it was lowest in human. While spleen  $V_T(-)$  was slightly lower than pancreas  $V_T(-)$  in baboon, spleen  $V_T(-)$  was substantially lower than pancreas  $V_T(-)$  and at a similar level to renal



cortex  $V_T(-)$  in human. In addition to species differences in parent tracer uptake, differences between baboon and human might be attributed to the difference in types of labeled metabolites and metabolite fraction in tissues. From *ex vivo* baboon studies, the metabolite fraction at 90 min post injection of [ $^{18}\text{F}$ ]FP(-)-DTBZ was 95 % in the plasma, 70 % in the renal cortex, 50 % in the spleen, and 40 % in the pancreas. The metabolite fraction in the plasma was lower (70 %) in human. However, the metabolite fractions in human organs cannot be measured.

We applied the kinetic models with and without blood volume correction to the TACs. Even though the blood volume fraction was large (up to 63 % in the spleen), a small reduction was observed in  $V_T$  with blood volume correction. Such a small difference is understood by considering the  $V_T$  under equilibrium condition, *i.e.*, the concentration ratio of tissue to metabolite-corrected plasma. For example, the spleen  $V_T$  with blood volume correction is described as  $\{C_{\text{tissue}} - \text{blood volume} \times C_{\text{whole blood}}\} / \{\text{parent fraction} \times C_{\text{plasma,unc}}\}$ , where “unc” refers to the plasma concentration uncorrected for metabolites. Since  $C_{\text{whole blood}}$  and  $C_{\text{plasma,unc}}$  were similar at later times post injection, the  $V_T$  in the spleen is  $\{C_{\text{tissue}} - 0.63 \times C_{\text{plasma,unc}}\} / \{0.3 \times C_{\text{plasma,unc}}\} = V_T(\text{spleen, without blood volume correction}) - 2.1$  (here, 0.3 represents the parent plasma fraction). Thus, the difference with/without blood volume correction is estimated as  $\sim 2 \text{ ml/cm}^3$ . The differences would be smaller in tissues with smaller blood volume.

In addition to the high affinity of [ $^{18}\text{F}$ ]FP-(+)-DTBZ with VMAT2, [ $^{18}\text{F}$ ]FP-(+)-DTBZ has a low affinity for sigma-1 receptors ( $K_i = 95 \text{ nM}$ ) [20]. The affinity for 44 other CNS and cardiovascular receptors was found to be even lower ( $\text{IC}_{50} > 10 \text{ }\mu\text{M}$ ) [20]. [ $^{18}\text{F}$ ]FP(-)-DTBZ also has a low affinity for sigma-1 receptors ( $K_i = 110 \text{ nM}$ ), which is similar to that of [ $^{18}\text{F}$ ]FP-(+)-DTBZ. In our baboon studies with a [ $^{18}\text{F}$ ]FP-(+)-DTBZ fluvoxamine displacement study [7], negligible changes were detected in SUV curves in the pancreas, renal cortex, and spleen. Hence, the results indicate the low-affinity sigma-1 receptor binding does not contribute to the binding in the renal cortex and spleen. Extrapolating from the results in baboons, it is expected that [ $^{18}\text{F}$ ]FP-(+)-DTBZ and its metabolites do not bind specifically with non-VMAT2 sites in the renal cortex and spleen in humans. Based on similar affinities for sigma-1 receptors, it is also expected that [ $^{18}\text{F}$ ]FP(-)-DTBZ negligibly binds to sigma-1 receptor. Since a [ $^{18}\text{F}$ ]FP(-)-DTBZ fluvoxamine displacement study has never been conducted, the affinity profile of the metabolites of [ $^{18}\text{F}$ ]FP(-)-DTBZ is not known.

We addressed two questions to quantify specific binding in the pancreas: (1) is non-displaceable uptake homogeneous among organs and (2) is non-displaceable uptake similar between enantiomers. For the first question, if non-displaceable uptake is uniform among organs,  $V_T(-)$  values of different organs are expected to be similar. However,  $V_T(-)$  in the pancreas was significantly higher than that in the spleen and renal cortex, so  $V_T(-)$  was not uniform among organs. Considering that tissue compositions including the blood volume contributions are different between organs, this is not a surprising result. For example, even if the uptake per unit extravascular volume is compatible in different organs, since the blood volumes differ substantially between organs (see above),  $V_{\text{ND}}$  values will differ. Therefore, it is not possible to directly select a reference tissue with the same non-displaceable uptake

as the pancreas. For the second question, since VMAT2 density is considered to be negligible in the renal cortex and spleen,  $V_T(-)$  was expected to be similar to  $V_T(+)$  in these regions. However,  $V_T(-)$  was significantly lower than  $V_T(+)$  in the renal cortex and spleen (for both regions, HC:  $P < 0.001$ , T1DM:  $P < 0.01$ ), while  $V_T(-)$  of the spleen was similar to that of the renal cortex. This suggests that non-displaceable uptake in tissue is different between [ $^{18}\text{F}$ ]FP-(+)-DTBZ and [ $^{18}\text{F}$ ]FP-(-)-DTBZ. Note that the plasma free fractions of the enantiomers were also substantially different; *i.e.*, they interact differently with proteins, so it is not surprising that nonspecific binding in tissue differs. Based on these results, non-displaceable uptake is different among organs and between the two enantiomers.

Since no ideal reference tissue exists, we explored normalization methods to compare VMAT2 binding between HC and T1DM groups. We applied three methods based on the baboon study [5]. The first method is a conventional one used in previous [ $^{18}\text{F}$ ]FP-(+)-DTBZ studies. It assumes that  $V_{ND}(+)$  is uniform among organs and used  $V_T(+)$  (or SUV(+)) of either the spleen or renal cortex as  $V_{ND}(+)$  (or reference SUV(+)). Since  $V_{T(+),\text{spleen}}$  was higher than  $V_{T(+),\text{renal cortex}}$  in both HC and T1DM groups (Table 2), pancreatic  $BP_{ND}(\text{ref}:\text{spleen})$  was lower than pancreatic  $BP_{ND}(\text{ref}:\text{renal cortex})$ . A significant difference in  $BP_{nd}$  between groups was observed with the spleen as a reference, but the difference in this small cohort was not statistically significant with the renal cortex as a reference. A significant difference in SUV<sub>R</sub>-1 was also observed only when the spleen was used as a reference. While this method is simple to apply, the inter-organ differences in  $V_T(-)$  call the assumption of method 1 into question.

The second method assumes uniform non-displaceable uptake of the two enantiomers and the use of pancreas  $V_T(-)$  as  $V_{ND}(+)$ . However, this approach requires PET imaging with both enantiomers for each subject. The group differences in  $BP_{nd}$  were not significant, and the between-group difference was smallest among the three methods. Furthermore, this second method is not applicable to SUV, since the input function of [ $^{18}\text{F}$ ]FP-(+)-DTBZ was lower than that of [ $^{18}\text{F}$ ]FP-(-)-DTBZ in both HC and T1DM groups (Fig. 2). Since SUV is affected by plasma clearance, we cannot simply use pancreas SUV(-) as a reference SUV to compare with pancreas SUV(+). Thus, the second method is not recommended.

For the third method, we hypothesized that the between-organ ratio ( $\alpha$ ) of  $V_{ND}$  is the same between enantiomers. In this way, different tissue compositions between organs, including differences in blood volume fraction, can affect non-displaceable uptake, but we assumed that it should affect the two enantiomers to the same degree. Since there was no significant group difference in the  $\alpha$  values, a ratio calculated from all subjects was used to calculate  $V_{ND}(+)$ . We also hypothesized that any radiometabolite contribution to the  $V_{ND}$  ratio is similar for both enantiomers. This is important since the plasma metabolite profiles of the two enantiomers were different (Fig. 1). In plasma, since radiometabolites were measured, a corrected input function was used in the modeling; thus, these differences in metabolites do not affect the  $V_{ND}$  values. In tissue, if the fraction of counts attributable to radiolabeled metabolites differed between the enantiomers in a given organ, our assumption would be incorrect. We have no data for tissue radiometabolite fraction in humans; however, we performed such measurements in non-human primate. Specifically, the tissue metabolite fractions in the pancreas and spleen were similar for both enantiomers ([ $^{18}\text{F}$ ]FP-(+)-DTBZ,

99 % (pancreas) and 94 % (spleen); [ $^{18}\text{F}$ ]FP-(-)- DTBZ, 56 % (pancreas) and 53 % (spleen)), as shown in Table 5 in [5]. The presence of radiolabeled metabolites in the tissue would cause an overestimation of the volume of distribution (the equilibrium ratios of tissue to plasma), with the magnitude of this effect based on the tissue metabolite fraction. Since we found that both (+)- and (-)- tracers had equal radiometabolite fractions in the pancreas and spleen, the overestimation of  $V_{\text{ND}}$  would be expected to be comparable for both tissues, and this effect would cancel out in calculating the between-organ  $V_{\text{ND}}$  ratio,  $\alpha$ .

The third method is applicable to SUV, and the population ratio calculated from SUV was similar to that from  $V_{\text{T}}$ . Since we used a population ratio,  $P$  values for group differences from method 3 were exactly the same as those from method 1 (Table 4). However, the between-group difference in pancreas  $BP_{\text{ND}}$  was the largest of all methods. The use of scaled  $V_{\text{T}(+, \text{spleen})}$  produced the largest group difference (75 % for  $BP_{\text{ND}}$ ; 85 % for SUV-1) and the smallest magnitude of pancreas  $BP_{\text{ND}}$  and SUV-1 in T1DM (0.40 for  $BP_{\text{ND}}$ ; 0.18 for SUV-1). Such low specific binding in the T1DM pancreas is consistent with the fact that functional BCM is almost completely depleted in T1DM patients. Comparing these results, method 3 with the spleen as a reference tissue was chosen as the suitable normalizing method.

Total tracer uptake in the pancreas (functional binding capacity, FBC) can be computed by multiplying  $BP_{\text{ND}}$  by the whole pancreas volume [9, 10, 21]. The population values of the pancreas were used for computation (HC 77.77 ml and T1DM 41.16 ml) [22]. Among all methods, method 3 with the spleen as a reference region gave the largest loss (87 %) of FBC in the T1DM group. The remaining 13 % FBC can be partly attributed to VMAT2 binding in the PP cells. This difference between groups is similar to the VMAT2-positive PP cell binding (7–10 %). We also compared the use of pancreas  $V_{\text{T}(+)}$  or SUV(+) to differentiate the two groups (Table 2). SUV(+) provided a smaller  $P$  value and bigger group differences than  $V_{\text{T}(+)}$ . This larger signal can be attributed to the fact that SUV reflects differences in the input function as well as differences in specific binding between groups. The HC input function was higher than that of T1DM (Fig. 2) for both enantiomers. Moreover, a significant group difference was observed in pancreas SUV(-), which is also affected by the between-group differences in plasma SUV. Since  $V_{\text{T}(+)}$  can account for the differences in the arterial input, pancreas  $V_{\text{T}(+)}$  is a more suitable parameter than SUV to differentiate groups, though a larger sample size is needed before completely excluding the utility of SUVs.

There was a trend towards lower pancreas  $V_{\text{T}(-)}$  in the T1DM group than in the HC group; this was not seen in the spleen or renal cortex. If non-specific binding is lower in the pancreas of T1DM patients, but not in the reference regions, this would cause an underestimation of  $BP_{\text{ND}}$  in the T1DM patients relative to HC. To quantitatively assess the potential impact of group difference in non-specific binding, we recalculated  $BP_{\text{ND}}$  with method 3 (spleen) using the group-averaged values of  $\alpha_{\text{spleen}}$ . In that case, the difference in  $BP_{\text{ND}}$  between HC and T1DM groups was reduced from 75 % (Table 3) to 42 %. To definitively address this issue, a larger cohort of patients would be needed.

Using the proposed method 3,  $BR_{ND}$  values are globally lower than those of previous publications using the kidney [9] or spleen [10] as a reference region, both in HC and T1DM groups. However, the reduction in  $BR_{ND}$  and FBC between HC and T1DM groups is now larger than that in previous publications. This larger reduction is more consistent with expectations, since T1DM patients have almost no remaining pancreatic beta cells. However, even with the larger percent reduction in  $BR_{ND}$ , the statistical significance of the between-group difference was not altered; this occurred because a single population value of  $\alpha$  was used in computing  $V_{ND}(+)$ .

## Conclusions

We compared the kinetics of [ $^{18}\text{F}$ ]FP-(+)-DTBZ and [ $^{18}\text{F}$ ]FP-(-)-DTBZ in healthy controls and type 1 diabetes mellitus subjects. The heterogeneity in distribution volumes and SUVs among organs and between enantiomers demonstrated that there is a need to scale uptake values from other organs to provide accurate estimates of non-displaceable uptake for quantification of VMAT2 in the pancreas. Moreover, SUV is affected by the differences in the plasma clearance between groups, and its use as quantitative outcome measures can thus be misleading. We conclude that  $BR_{ND}$  computed using scaled spleen values for non-displaceable uptake is a suitable method for quantification of VMAT2 binding in the pancreas.

## Supplementary Material

Refer to Web version on PubMed Central for supplementary material.

## Acknowledgements

The authors appreciate the excellent technical assistance of the staff at the Yale University PET Center.

*Funding Information.* This study was sponsored by the Juvenile Diabetes Research Foundation 37-2011-633. This work was also made possible by 1S10OD010322-01 and by CTSA Grant Number UL1 TR000142 from the National Center for Advancing Translational Sciences (NCATS), a component of the National Institutes of Health (NIH). Its contents are solely the responsibility of the authors and do not necessarily represent the official view of NIH.

## References

1. Anlauf M, Eissele R, Schafer MK et al. (2003) Expression of the two isoforms of the vesicular monoamine transporter (VMAT1 and VMAT2) in the endocrine pancreas and pancreatic endocrine tumors. *J Histochem Cytochem* 51(8): 1027–1040. 10.1177/002215540305100806 [PubMed: 12871984]
2. Harris PE, Ferrara C, Barba P, Polito T, Freeby M, Maffei A (2008) VMAT2 gene expression and function as it applies to imaging betacell mass. *J Mol Med (Berl)* 86(1):5–16. 10.1007/s00109-007-0242-x [PubMed: 17665159]
3. Maffei A, Liu Z, Witkowski P, Moschella F, Pozzo GD, Liu E, Herold K, Winchester RJ, Hardy MA, Harris PE (2004) Identification of tissue-restricted transcripts in human islets. *Endocrinology* 145(10):4513–4521. 10.1210/en.2004-0691 [PubMed: 15231694]
4. Saisho Y, Harris PE, Butler AE, Galasso R, Gurlo T, Rizza RA, Butler PC (2008) Relationship between pancreatic vesicular monoamine transporter 2 (VMAT2) and insulin expression in human pancreas. *J Mol Histol* 39(5):543–551. 10.1007/s10735-008-9195-9 [PubMed: 18791800]

5. Naganawa M, Lin SF, Lim K, Labaree D, Ropchan J, Harris P, Huang Y, Ichise M, Carson RE, Cline GW (2016) Evaluation of pancreatic VMAT2 binding with active and inactive enantiomers of 18F-FP-DTBZ in baboons. *Nucl Med Biol* 43(12):743–751. 10.1016/j.nucmedbio.2016.08.018 [PubMed: 27673755]
6. Rahier J, Goebbels RM, Henquin JC (1983) Cellular composition of the human diabetic pancreas. *Diabetologia* 24(5):366–371 [PubMed: 6347784]
7. Kung MP, Hou C, Lieberman BP, Oya S, Ponde DE, Blankemeyer E, Skovronsky D, Kilbourn MR, Kung HF (2008) In vivo imaging of beta-cell mass in rats using 18F-FP-(+)-DTBZ: a potential PET ligand for studying diabetes mellitus. *J Nucl Med* 49(7):1171–1176. 10.2967/jnumed.108.051680 [PubMed: 18552132]
8. Harris PE, Farwell MD, Ichise M (2013) PET quantification of pancreatic VMAT 2 binding using (+) and (–) enantiomers of [18F]FP-DTBZ in baboons. *Nucl Med Biol* 40(1):60–64. 10.1016/j.nucmedbio.2012.09.003 [PubMed: 23102539]
9. Normandin MD, Petersen KF, Ding YS, Lin SF, Naik S, Fowles K, Skovronsky DM, Herold KC, McCarthy TJ, Calle RA, Carson RE, Treadway JL, Cline GW (2012) In vivo imaging of endogenous pancreatic beta-cell mass in healthy and type 1 diabetic subjects using F-18-fluoropropyl-dihydrotrabenazine and PET. *J Nucl Med* 53(6):908–916. 10.2967/jnumed.111.100545 [PubMed: 22573821]
10. Freeby MJ, Kringas P, Goland RS, Leibel RL, Maffei A, Divgi C, Ichise M, Harris PE (2016) Cross-sectional and test-retest characterization of PET with [18F]FP-(+)-DTBZ for beta cell mass estimates in diabetes. *Mol Imaging Biol* 18(2):292–301. 10.1007/s11307-015-0888-7 [PubMed: 26370678]
11. Singhal T, Ding YS, Weinzimmer D, Normandin MD, Labaree D, Ropchan J, Nabulsi N, Lin SF, Skaddan MB, Soeller WC, Huang Y, Carson RE, Treadway JL, Cline GW (2011) Pancreatic beta cell mass PET imaging and quantification with [nC]DTBZ and [18F]FP-(+)-DTBZ in rodent models of diabetes. *Mol Imaging Biol* 13(5):973–984. 10.1007/s11307-010-0406-x [PubMed: 20824509]
12. Kung MP, Hou C, Goswami R, Ponde DE, Kilbourn MR, Kung HF (2007) Characterization of optically resolved 9-fluoropropyl-dihydrotrabenazine as a potential PET imaging agent targeting vesicular monoamine transporters. *Nucl Med Biol* 34(3):239–246. 10.1016/j.nucmedbio.2006.12.005 [PubMed: 17383573]
13. Watabe H, Endres CJ, Breier A, Schmall B, Eckelman WC, Carson RE (2000) Measurement of dopamine release with continuous infusion of [<sup>11</sup>C]raclopride: optimization and signal-to-noise considerations. *J Nucl Med* 41(3):522–530 [PubMed: 10716328]
14. Pavlidis T (1982) Algorithms for graphics and image processing. *Computer Science*, DOI: 10.1007/978-3-642-93208-3
15. Ichise M, Toyama H, Innis RB, Carson RE (2002) Strategies to improve neuroreceptor parameter estimation by linear regression analysis. *J Cereb Blood Flow Metab* 22(10):1271–1281. 10.1097/01.WCB.0000038000.34930.4E [PubMed: 12368666]
16. Innis RB, Cunningham VJ, Delforge J, Fujita M, Gjedde A, Gunn RN, Holden J, Houle S, Huang SC, Ichise M, Iida H, Ito H, Kimura Y, Koeppe RA, Knudsen GM, Knuuti J, Lammertsma AA, Laruelle M, Logan J, Maguire RP, Mintun MA, Morris ED, Parsey R, Price JC, Slifstein M, Sossi V, Suhara T, Votaw JR, Wong DF, Carson RE (2007) Consensus nomenclature for in vivo imaging of reversibly binding radioligands. *J Cereb Blood Flow Metab* 27(9):1533–1539. 10.1038/sj.jcbfm.9600493 [PubMed: 17519979]
17. Arikawa S, Uchida M, Kunou Y, Kaida H, Uozumi J, Hayabuchi N, Okabe Y, Murotani K (2012) Assessment of chronic pancreatitis: use of whole pancreas perfusion with 256-slice computed tomography. *Pancreas* 41(4):535–540. 10.1097/MPA.0b013e3182374fe0 [PubMed: 22228048]
18. Anderson H, Yap JT, Wells P, Miller MP, Propper D, Price P, Harris AL (2003) Measurement of renal tumour and normal tissue perfusion using positron emission tomography in a phase II clinical trial of razoxane. *Br J Cancer* 89(2):262–267. 10.1038/sj.bjc.6601105 [PubMed: 12865914]
19. Koeppe RA, Frey KA, Kuhl DE, Kilbourn MR (1999) Assessment of extrastriatal vesicular monoamine transporter binding site density using stereoisomers of [11C]dihydrotrabenazine. *J Cereb Blood Flow Metab* 19(12):1376–1384. 10.1097/00004647-199912000-00011 [PubMed: 10598942]

20. Tsao HH, Skovronsky DM, Lin KJ, Yen TC, Wey SP, Kung MP (2011) Sigma receptor binding of tetrabenazine series tracers targeting VMAT2 in rat pancreas. *Nucl Med Biol* 38(7):1029–1034. 10.1016/j.nucmedbio.2011.03.006 [PubMed: 21982574]
21. Goland R, Freeby M, Parsey R, Saisho Y, Kumar D, Simpson N, Hirsch J, Prince M, Maffei A, Mann JJ, Butler PC, van Heertum R, Leibel RL, Ichise M, Harris PE (2009) <sup>11</sup>C-dihydrotrabenazine PET of the pancreas in subjects with long-standing type 1 diabetes and in healthy controls. *J Nucl Med* 50(3):382–389. 10.2967/jnumed.108.054866 [PubMed: 19223416]
22. Virostko J, Hilmes M, Eitel K, Moore DJ, Powers AC (2016) Use of the electronic medical record to assess pancreas size in type 1 diabetes. *PLoS One* 11(7):e0158825 10.1371/journal.pone.0158825 [PubMed: 27391588]

Author Manuscript

Author Manuscript

Author Manuscript

Author Manuscript



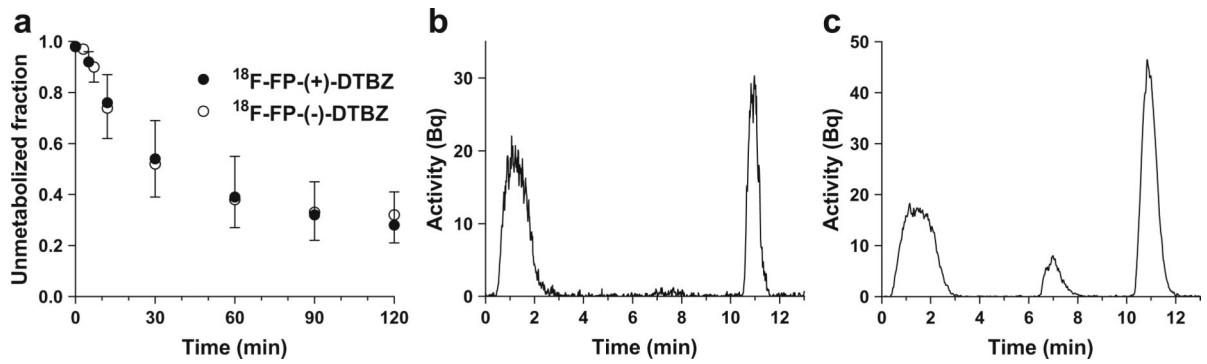


**Fig. 1.**

**a** Mean  $\pm$  SD of unmetabolized fraction in the plasma of [ $^{18}\text{F}$ ]FP-(+)-DTBZ (closed circles,  $n = 10$ ) and [ $^{18}\text{F}$ ]FP-(-)-DTBZ (open circles,  $n = 10$ ). Representative HPLC chromatograms of plasma at 60 min after injection of **b** [ $^{18}\text{F}$ ]FP-(+)-DTBZ and **c** [ $^{18}\text{F}$ ]FP-(-)-DTBZ in a healthy subject.

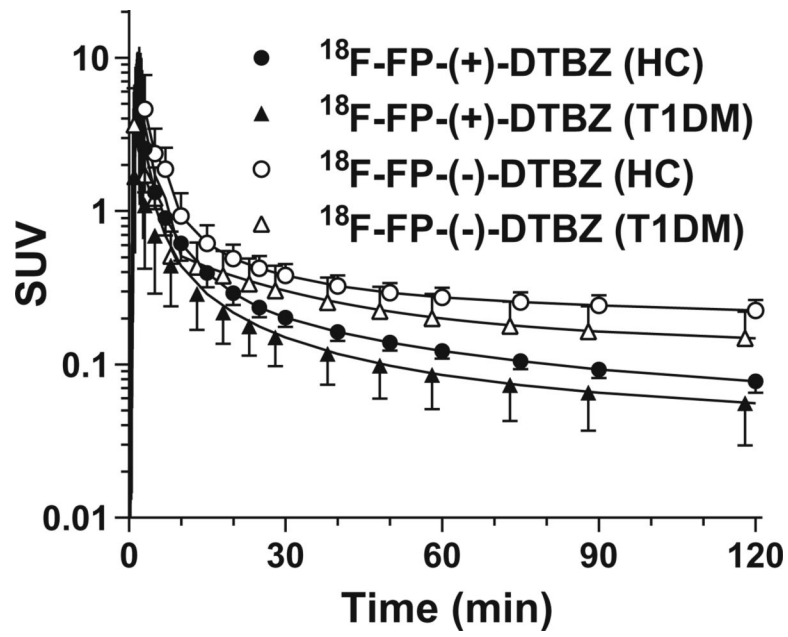


**Fig. 2.** Mean  $\pm$  SD of metabolite-corrected plasma curves of [ $^{18}\text{F}$ ]FP-(+)-DTBZ (closed symbols) and [ $^{18}\text{F}$ ]FP-(-)-DTBZ (open symbols). Healthy subjects and T1DM patients are shown in circles and triangles, respectively.

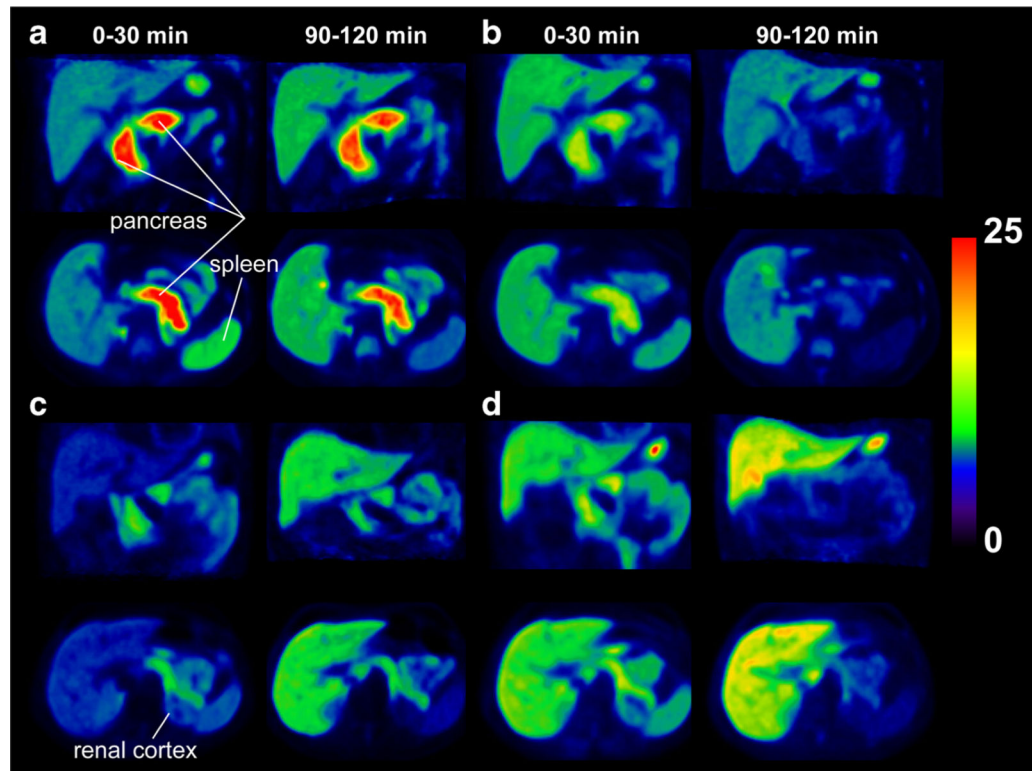


**Fig. 3.** PET SUV images of [ $^{18}\text{F}$ ]FP-(+)-DTBZ (**b, c**) and [ $^{18}\text{F}$ ]FP-(-)-DTBZ (**b, d**) from a healthy subject (**a, b**) and a T1DM patient (**c, d**). PET images were summed from 0 to 30 and from 90 to 120 min post injection.

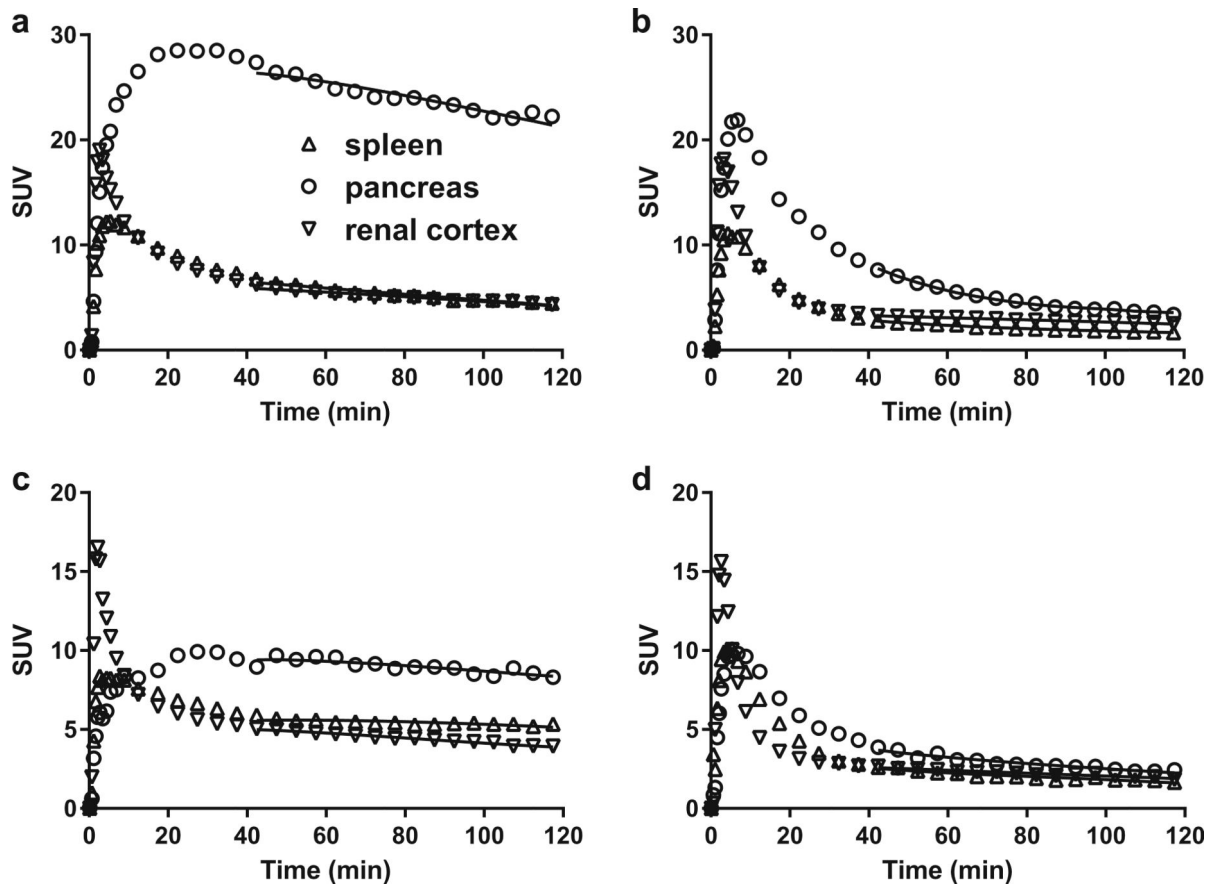


**Fig. 4.** Examples of regional time-activity curves [ $^{18}\text{F}$ ]FP-(+)-DTBZ (**a, c**) and [ $^{18}\text{F}$ ]FP-(-)-DTBZ (**b, d**) in healthy subjects (**a, b**) and T1DM patients (**c, d**). Solid curves show the fits obtained with multilinear analysis 1.

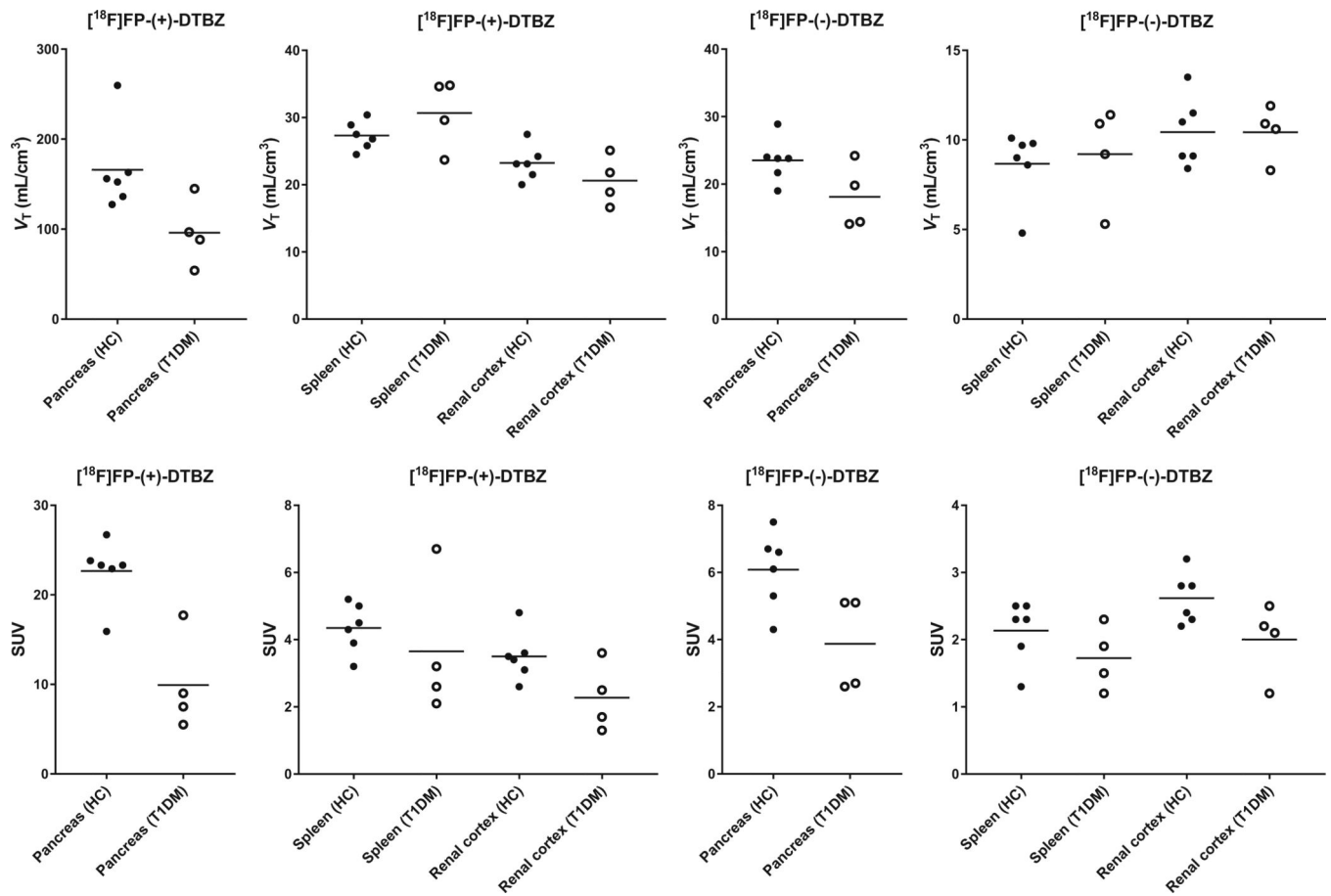


**Fig. 5.** Scatter plots of distribution volume and SUVs in different groups. Closed and open circles denote healthy controls and T1DM patients, respectively.

Table 1.

Injection parameters

Parameter	HC (n = 6)		TIDM (n = 4)	
	[ <sup>18</sup> F]FP-(+)-DTBZ	[ <sup>18</sup> F]FP-(-)-DTBZ	[ <sup>18</sup> F]FP-(+)-DTBZ	[ <sup>18</sup> F]FP-(-)-DTBZ
Age (years)	30 ± 6		31 ± 2	
Body weight (kg)	85.9 ± 8.8		77.2 ± 6.7	
Injected mass (nmol)	2.9 ± 2.4	1.6 ± 1.0	1.7 ± 0.7	1.5 ± 1.0
Specific activity at the time of injection (MBq/nmol)	179 ± 130	219 ± 86	173 ± 37	203 ± 99
Plasma free fraction	0.20 ± 0.02	0.33 ± 0.02	0.21 ± 0.02	0.35 ± 0.03



Table 2.

Distribution volume ( $V_T$ ) and SUVs

Regions	$V_T$ (ml/cm <sup>3</sup> )	SUV										
		$[^{18}\text{F}]\text{FP}-(+)\text{-DTBZ}$		$[^{18}\text{F}]\text{FP}-(+)\text{-DTBZ}$		$[^{18}\text{F}]\text{FP}-(+)\text{-DTBZ}$						
	HC	TIDM	P value	HC	TIDM	P value	HC	TIDM	P value			
Pancreas	166 ± 48	96 ± 37	0.04	24 ± 3	18 ± 5	0.06	22.6 ± 3.6	9.9 ± 5.4	0.002	6.1 ± 1.1	3.9 ± 1.5	0.03
Spleen	27 ± 2	31 ± 5	0.19	9 ± 2	9 ± 3	0.72	4.3 ± 0.7	3.7 ± 2.1	0.47	2.1 ± 0.5	1.7 ± 0.5	0.22
Renal cortex	23 ± 3	21 ± 4	0.22	10 ± 2	10 ± 2	0.98	3.5 ± 0.7	2.3 ± 1.0	0.05	2.6 ± 0.4	2.0 ± 0.6	0.07

$V_T$  values were derived from the MA1 model, and SUVs were calculated from 60 to 120 min post injection. Values are expressed as mean±SD for healthy controls (HC,  $n = 6$ ) and T1DM patients ( $n = 4$ ). Group differences were tested using the *t* test

Table 3.

Non-displaceable distribution volume ( $V_{ND}$ ) and pancreatic  $BP_{ND}$

Method	$V_{ND}$		$\alpha$		Pancreatic $BP_{ND}$				
	HC	TIDM	HC	TIDM	All subjects	HC	TIDM	P value	% difference
1. $V_T(+, \text{spleen})$	27 (8)	31 (17)				5.0 (27)	2.2 (55)	0.01	56
2. $V_T(+, \text{renal cortex})$	23 (11)	21 (18)				6.2 (32)	3.8 (51)	0.10	38
3. $V_T(-, \text{pancreas})$	24 (14)	18 (26)				6.3 (50)	4.3 (40)	0.29	31
4. $V_T(+, \text{spleen})/\alpha_{\text{spleen}}$	62 (8)*	70 (17)*	0.37 (25)	0.54 (40)	0.44 (38)	1.6 (36)*	0.40 (132)*	0.01	75
5. $V_T(+, \text{renal cortex})/\alpha_{\text{renal}}$	46 (11)*	41 (18)*	0.45 (21)	0.60 (27)	0.51 (28)	2.7 (38)*	1.5 (68)*	0.10	45

$V_{ND}$  values and  $\alpha$  ratios were derived from the MA1  $V_T$  values using three methods. See text for details. Data are expressed as mean (COV%). Group differences in pancreatic  $BP_{ND}$  were compared using  $t$  test

\*  $\alpha_{\text{spleen}}$  and  $\alpha_{\text{renal}}$  from all subjects were used to calculate  $V_{ND}$  and  $BP_{ND}$

Table 4.

Reference SUV and pancreatic SUV<sub>R-1</sub>

Method	Reference SUV		$\alpha$		Pancreatic SUV <sub>R-1</sub>				P value	% difference
	HC	TIDM	HC	TIDM	All subjects	HC	TIDM	HC		
1. SUV(+,spleen)	4.3 (17)	3.7 (57)				4.3 (16)	1.8 (46)	4.3 (16)	0.001	57
2. SUV(+,renal cortex)	3.5 (21)	2.3 (46)				5.6 (21)	3.6 (45)	5.6 (21)	0.056	35
3. SUV(+,spleen)/ $\alpha_{\text{spleen}}$	10 (17)*	8.8 (57)*	0.36 (26)	0.50 (41)	0.41 (37)	1.2 (23)*	0.18 (197)*	1.2 (23)*	0.001	85
4. SUV(+,renal cortex)/ $\alpha_{\text{renal}}$	7.2 (21)*	4.6 (46)*	0.45 (25)	0.55 (31)	0.49 (28)	2.2 (26)*	1.2 (63)*	2.2 (26)*	0.056	44

IND values and  $\alpha$  ratios were derived from SUVs using methods 1 and 3. See text for details. Data are expressed as mean (COV%). Group differences in pancreatic SUV<sub>R-1</sub> were compared using *t* test

\*  $\alpha_{\text{spleen}}$  and  $\alpha_{\text{renal}}$  from all subjects were used for calculation